Chemical Engineering and Processing 50 (2011) 519–524

Contents lists available at ScienceDirect

Chemical Engineering and Processing: Process Intensification

journal homepage: www.elsevier.com/locate/cep

Wave interactions on a viscous film coating a vertical fibre: Formation of bound states

C. Duprat [a], D. Tseluiko [b], S. Saprykin [b], S. Kalliadasis [b], F. Giorgiutti-Dauphiné [a,*]

[a] CNRS, Univ Pierre et Marie Curie, Univ Paris-Sud, Lab FAST, Bat 502, Campus Univ, Orsay 91405, France
[b] Department of Chemical Engineering, Imperial College London, London SW7 2AZ, United Kingdom

ARTICLE INFO

Article history:
Received 21 February 2010
Received in revised form 27 August 2010
Accepted 12 October 2010
Available online 19 October 2010

PACS:
47.20.Ma
47.35.Fg
47.54.−r

Keywords:
Interfacial instabilities
Solitary waves
Pattern formation
Thin liquid films

ABSTRACT

Fibre coating has attracted considerable attention over the past years due to its engineering applications as well as fundamental interest generated by the fascinating complexity of the resulting flow. A liquid film coating axisymmetrically a vertical fibre and flowing under the action of gravity spontaneously breaks up into a regular drop-like wave train. This instability results primarily from the capillary pressure induced by the azimuthal curvature (Rayleigh–Plateau instability) while the pressure induced by the axial curvature has a stabilising effect. Streamwise viscous diffusion plays a dispersive role that dramatically affects the waves selection, speeds and shapes. When both surface tension and viscosity effects are strong, complex wave interactions lead to the formation of bound states. In this study, we investigate experimentally the details of those interactions and show that regular patterns of bound states can be obtained by external forcing. A qualitative theoretical explanation of the experimental findings is provided with a simple model for the flow.

1. Introduction

Fibre coating has attracted considerable attention over the past years due to its engineering applications as well as fundamental interest generated by the fascinating complexity of the resulting flow [1,2]. A liquid film coating axisymmetrically a vertical stationary fibre and flowing under the action of gravity spontaneously breaks up into a regular drop-like wave train [3]. This instability results primarily from the capillary pressure induced by the azimuthal curvature (Rayleigh-Plateau instability) while the pressure induced by the axial curvature has a stabilising effect. Streamwise viscous diffusion plays a dispersive role that dramatically affects the waves selection, speeds and shapes [4]. When both surface tension and viscosity effects are strong, complex wave interactions lead to the formation of bound states [5]. In this study, we investigate experimentally the details of those interactions and show that regular patterns of bound states can be obtained by external forcing. A qualitative theoretical explanation of the experimental findings is provided with a simple model for the flow.

2. Experiments

The experimental set-up consists of a vertical nylon fibre on which Rhodorsil silicon oil (density $\rho = 963$ kg/m^3, dynamic viscosity $\mu = 48 \times 10^{-3}$ Pa s, surface tension $\gamma = 20.8 \times 10^{-3}$ N/m at 25 °C) flows axisymmetrically [6] (Fig. 1(a)). Fibre radii R are small compared to the capillary length ($\kappa^{-1} = \sqrt{\gamma/(\rho g)} = 1.5$ mm) to ensure strong curvature effects, i.e. $0.23 < R\kappa < 0.3$. Notations are given in Fig. 1(c). The vertical downward axis x denotes the position on the fibre (with $x = 0$ at the inlet), r denotes the radial coordinate, and the free surface is given by $r = R + h(x, t)$. Just after the inlet, the film is of uniform thickness h_0 (Fig. 1(b)). The relevant dimensionless parameters are the Reynolds number $Re = \rho U_0 h_0/\mu$ and the Weber number $We = \gamma/\rho U_0^2 h_0$, where $U_0 = \rho g h_0^2/2\mu$ is a characteristic speed corresponding to a simple balance between viscous drag and gravity. Parameters are chosen in order to have both strong viscosity and surface tension effects ($Re \lesssim 1$, $We \sim 10$), that is 0.55 mm $< h_0 <$ 0.95 mm. In [5], we have introduced an additional non-trivial dimensionless parameter measuring the relative importance of dispersive effects defined as $\delta = 6/We\,Re\,A^{1/2}$, where $A = 8/5We + (h_0/R)^2$. This parameter compares the relative importance of surface tension and viscosity. In our experiments, $\delta \sim 0.5$. Under these conditions, the system behaves as a "noise amplifier": the advection of the waves by the flow dominates over the Rayleigh-Plateau instability, while the curvature effects are still important [3,6].

* Corresponding author.
E-mail address: fred@fast.u-psud.fr (F. Giorgiutti-Dauphiné).

0255-2701/$ – see front matter © 2010 Elsevier B.V. All rights reserved.
doi:10.1016/j.cep.2010.10.004

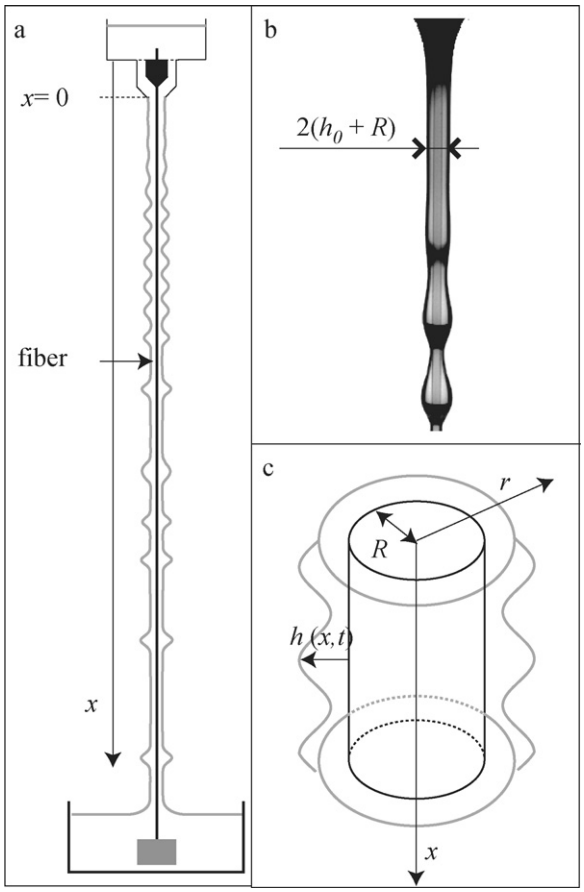

Fig. 1. (a) Experimental setup, (b) snapshot of the flow just after the inlet (R = 0.2 mm, h_0 = 0.55 mm), and (c) notations.

The natural (noise driven) evolution is depicted in Fig. 2. Such spatio-temporal diagrams are obtained with a linear camera following a vertical pixel line (parallel to the flow) with time, the dark lines tracking the trajectories of the wave peaks. After a few centimeters where the thickness remains constant, the film spontaneously breaks up into a regular wave train. This primary wave train is then destabilized (after 20–40 cm) through numerous coalescence events (Fig. 2(a)–A) where two droplets merge to form a larger, faster wave. After a certain distance on the fibre (typically 60 cm), no more coalescence occurs. We can then observe strong repulsions (Fig. 2(a)–B) where waves exchange fluid. This behaviour can be easily deduced from the peak lines on the spatio-temporal diagram. As the upstream faster wave (noted 1) approach the downstream slower wave (noted 2), fluid is drained from 1 to 2, leading to a decrease in the volume (hence a deceleration) of 1 and an increase in the volume (hence an acceleration) of 2, so that the waves repel one another.

The exchange of fluid between waves adjusts their size accordingly, and saturated waves are formed after a certain distance on the fibre (typically 80–100 cm). As noted from the quasi-parallel stripes on the spatiotemporal diagram, these solitary pulses have a nearly identical speed and an identical shape. Measurements at x = 1.4 m reveal an average deviation of 1–2% on the speed. These pulses can be referred to as "dissipative solitons" [7] that arise from a precise balance between nonlinearity, energy input/instability and energy output/dissipation. At the bottom of the fibre (Fig. 2(b)), the pulses merely rearrange through weak interactions with their neighbors. Pulses either attract (Fig. 2(b)–C) or repel (Fig. 2(b)–D) each other until they are at a specific distance which then remains constant while they travel at a constant speed. The two pulses then behave as a single object, forming a so called "bound state". Formation of bound states occurs in a wide variety of physical settings, from quantum mechanics to biological systems, complex fluids and pattern formation [8]. We note that as pulses interact only with their immediate neighbors, they can form 2-pulse (Fig. 2(b)–C) or 3-pulse (Fig. 2(b)–D) bound states.

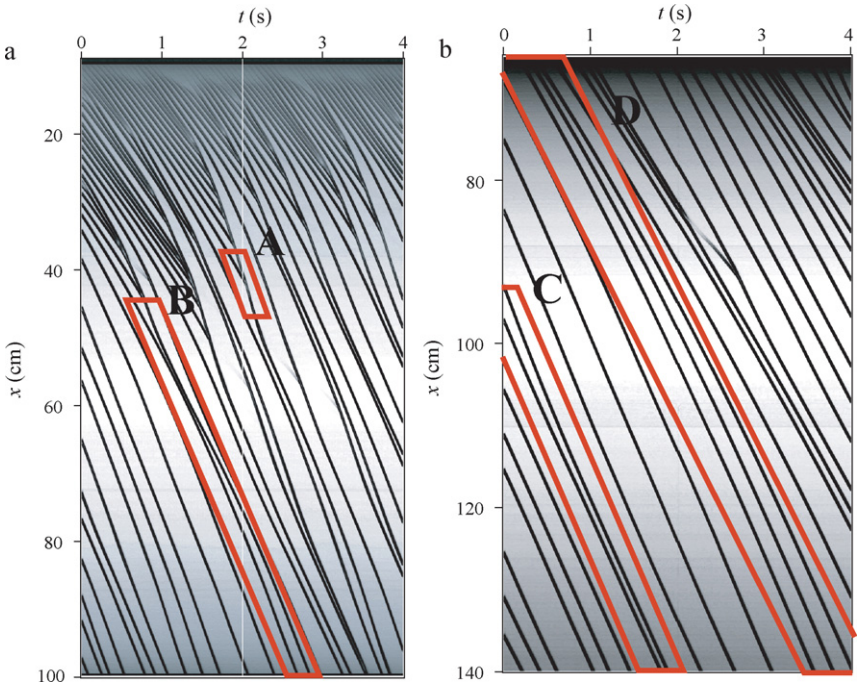

Fig. 2. Experimentally obtained spatio-temporal diagrams tracking the wave peaks during noise-driven evolution for R = 0.35 mm, h_0 = 0.85 mm (Re = 1.2, We = 5, δ = 0.4) (a) for 10 cm < x < 100 cm with A coalescence and B repulsion with mass transfer, and (b) for 65 cm < x < 140 cm with C attraction and D repulsion.

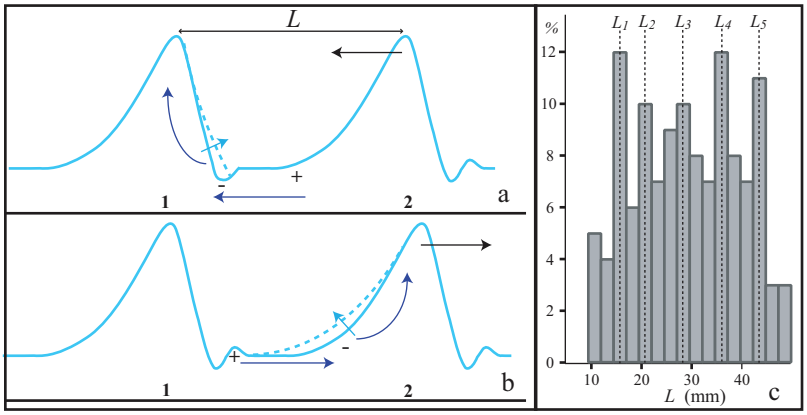

Fig. 3. Interaction mechanims: (a) attraction, (b) repulsion, (c) histogram of the separation distances L between successive pulses at the bottom of the fibre (1.2 m < x < 1.4 m) for R = 0.45 mm, h_0 = 0.74 mm (Re = 0.8, We = 10, δ = 0.44).

The dominant interaction mechanism is the overlap of the tails of neighboring pulses, as depicted in Fig. 3. Interactions are then strongly dependent on the shape of the pulse. Pulses have a steep front due to the non-linear kinematic effect which is preceded by a few capillary ripples arising from surface tension and damped by viscous friction. Viscous drag and gravity are responsible for the smooth monotonic tail [5]. As two pulses approach each other, the back slope of the front pulse experiences a positive (negative) differential pressure in the liquid as it overlaps with a maximum (minimum) of one of the capillary waves. This elevates (depresses) the back slope of the front pulse and decreases (increases) its curvature. The generated differential capillary pressure then causes the front pulse to move backwards (forwards) in a quasi-steady manner. This mechanism suggests the existence of several possible distances between pulses, depending on their initial separation distance and on the period of the capillary ripples. These distances should also have a common factor related to the period of the capillary ripples. Due to this slow interaction process, the system then heads towards reorganization, though no obvious regularity is observed. Nevertheless, statistics on the distances between pulses performed at the bottom of the fibre and with a large number of pulses, reveals that the system appears to select a finite number of distances at large times. The long-time distance distribution is presented on the histogram in Fig. 3(c). We can then note that five distances arise: $L_1 = 15.7 \pm 1.3$ mm, $L_2 = 20.7 \pm 1.3$ mm, $L_3 = 27 \pm 2.5$ mm, $L_4 = 37 \pm 2.5$ mm and $L_5 = 43.4 \pm 1.3$ mm. These prominent separation distances also have a common factor ($L_{i+1} - L_i \approx 6$) as suggested by the above physical mechanism.

To capture the specific pulse separation distances, we can reduce the initial distance distribution by imposing a weak forcing at the inlet. Forcing is achieved by creating pressure modulations in the upper tank [6]. The forcing signal competes with the amplification of the ambient (white) noise. Low-amplitude forcing then gives rise to a modulated signal at inlet containing many harmonics. We obtain a periodic signal where the separation distances and the wave amplitudes show small deviations from a mean value. A typical signal measured at x = 5 cm is presented in Fig. 4: the liquid film exhibits periodic undulations at a frequency f_0 = 12 Hz modulated with a carrier frequency Δf = 3 Hz. The thickness deviates from its mean value h_0 with fluctuations up to 20%. We can then impose the initial distances between pulses while letting the system relax to its equilibrium as the waves grow. The inlet signal (hence the initial distance distribution) can be controlled by adjusting both frequency and amplitude of the forcing device. Note that low frequency and/or high amplitude forcing lead to the synchronization of the flow with the forcing frequency [6]. By imposing a weak forcing, we observe that the transient destabilization regime is skipped, and bound states form rapidly. Such a phenomenon is presented in Fig. 5 (for the same parameters as for Fig. 2). We indeed obtain waves that quickly group into packets via both attractions and repulsions. The packets are formed of mostly two (Fig. 5(a) and (b)) or three (Fig. 5 (c) and (d)) pulses. The resulting pattern depends on the forcing signal frequency and modulation, and can be easily tuned on. Statistical analysis reveals that the system then selects two distances, whose values correspond to the ones obtained without forcing. For the example given in Fig. 5, the 2-pulse bound state is characterized by $L_{1'} = 14.5 \pm 0.7$ mm $= L_1$ and $L_{3'} = 26 \pm 1$ mm $= L_3$, while the 3-pulse bound state is characterized by $L_{1'} = 14.5 \pm 0.6$ mm $= L_1$ and $L_{2'} = 20.3 \pm 0.6$ mm $= L_2$. Depending on the inlet signal (i.e. the initial distances between waves), pulses attract or repel, and the system selects two distances or more between its intrinsic specific distances. When the system selects three distances, more complicated patterns can arise (such as 2 pulses – 1 pulse – 2 pulses arrangement). Hence, forcing allows us to capture the specific distances already present in the system.

Furthermore, the selected pattern remains periodic and steady all along the fibre. Regular arrangement can then be obtained very easily and in a reproducible manner. This also allows for a precise study of the interaction mechanism, as the interactions occur at a constant location on the fibre. An example of the formation of a

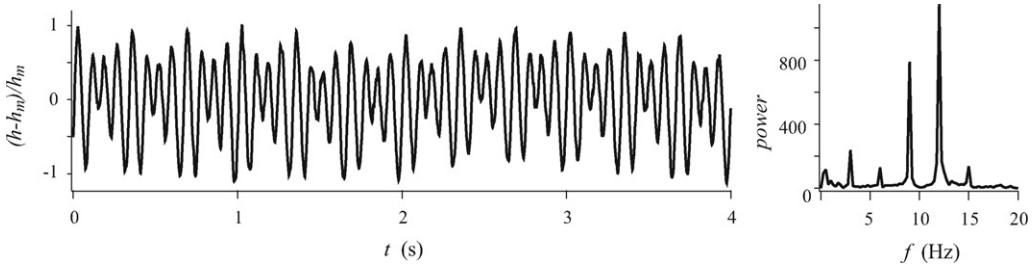

Fig. 4. Normalized inlet signal and corresponding spectra when imposing a weak forcing, measured at x = 5 cm for R = 0.475 mm, h_0 = 0.82 mm (Re = 1, We = 6, δ = 0.5).

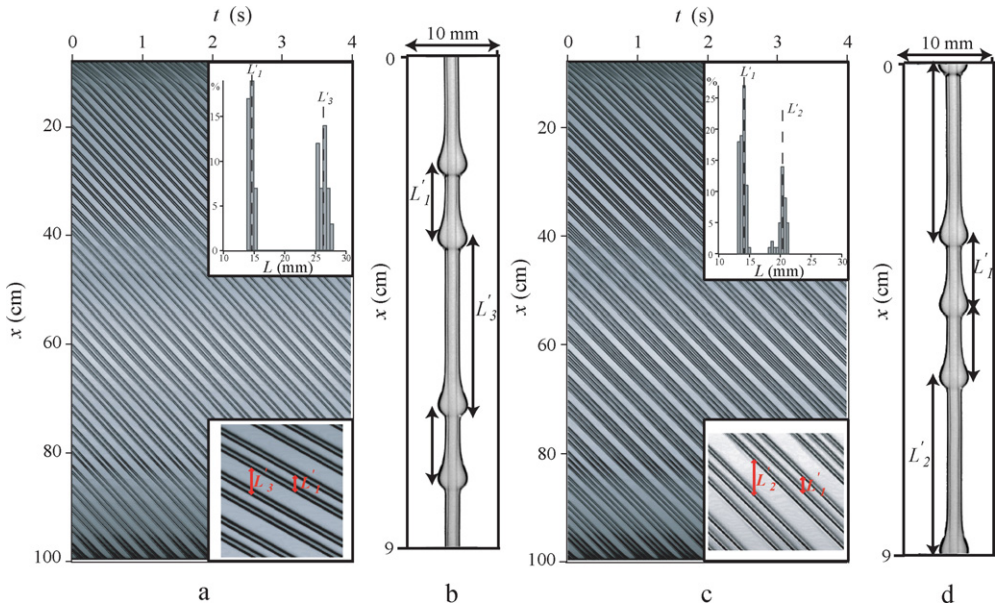

Fig. 5. Experimentally obtained forced bound states for $R = 0.45$ mm, $h_N = 0.74$ mm ($Re = 0.8$, $We = 10$, $\delta = 0.44$): snapshots taken at $x \sim 90$ cm, spatio-temporal diagrams and histograms of the separation distances L between successive pulses at the bottom of the fibre ($1.2\text{ m} < x < 1.4\text{ m}$) for (a, b) 2-pulse bound state and (c, d) 3-pulse bound state.

3-pulse bound states is given in Fig. 6. Initially, the signal is periodic and modulated, exhibiting uneven packets of three pulses as presented in Fig. 6(a). This pattern is periodically reproduced. The pulses have an amplitude 0.8 ± 0.03 mm (with small deviations, $h = 0.77$, 0.79 and 0.83 mm) and corresponding speed 6.2 ± 0.6 cm/s (5.6, 6.3 and 6.8 cm/s). The two downstream pulses then repel each other by exchanging a small amount of fluid through the substrate as is evident from the change in the amplitude of the pulses and the substrate thickness (Fig. 6(b)). Another repulsion occurs between the upstream and the following pulse; again, a small exchange of fluid can be noticed. These interactions lead to the formation of a bound state (Fig. 6(c)) with speed 6.2 cm/s and amplitude 0.79 mm separated by a constant distance $L = 5$ mm and riding on a flat substrate of thickness 0.23 mm. This regular pattern is periodically reproduced, with a constant distance between successive 3-pulse packets. Similar observations can be made for 2-pulse bound state, in agreement with our proposed interaction mechanism.

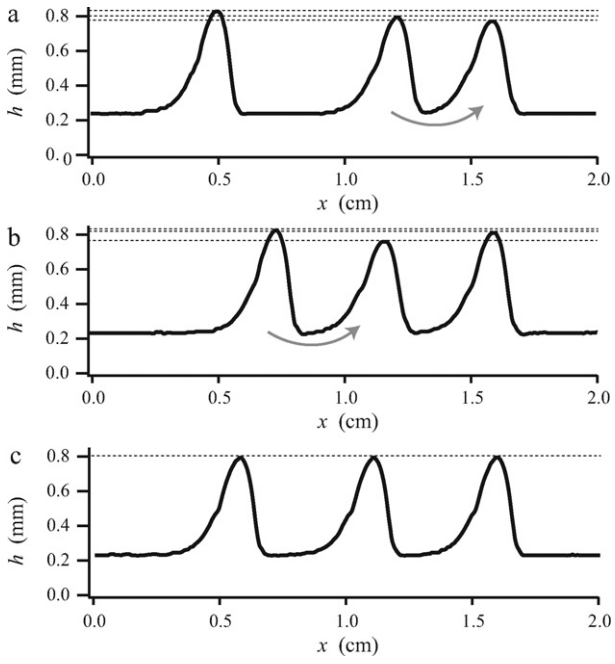

Fig. 6. Experimental profiles showing the formation of a 3-pulse bound state: (a) initial arrangement of the pulses, (b) intermediate positions of the pulses and (c) final pattern, for $R = 0.475$ mm, $h_0 = 0.82$ mm ($Re = 1$, $We = 6$, $\delta = 0.5$). Grey arrows represent the movement of fluid, while dotted lines indicate the amplitude of the pulses.

3. Coherent structure theory and regime map

In [5], we have derived a simple equation for the flow through a weakly nonlinear expansion of the base equations (Navier–Stokes in cylindrical coordinates together with the wall and the free-surface boundary conditions). We assumed $R/h_0 = O(\varepsilon^{-1})$, $We = O(\varepsilon^{-2})$ and $Re = O(\varepsilon)$, where $\varepsilon \ll 1$ is the long-wave/film parameter, which in thin-film flows is typically defined as the ratio of h_0 to a lengthscale over which streamwise variations occur. The amplitude deviation from h_0 is taken of $O(\varepsilon^2)$. We obtained the following equation:

$$H_T - c_\delta H_X + HH_X + H_{XX} + \delta H_{XXX} + H_{XXXX} = 0 \tag{1}$$

already in a frame moving with the velocity c_δ of a pulse. X, T, and H are defined through

$$x = h_0 A^{-1/2}(X + c_\delta T) + 3B\left[2 + \frac{2}{3}\alpha - \frac{1}{2}\alpha^2\right]T \tag{2}$$

$$t = 3U_0^{-1}BT, \quad H = 12A^{1/2}Bh_0^{-2}(h - h_0) \tag{3}$$

where $A = 8/5We + \alpha^2$, $B = h_0/We\,Re\,A^2$, and $\alpha = h_0/R$. Eq. (1) is the so-called "generalized Kuramoto–Shivashinsky" (gKS) equation. This equation has been postulated in the literature as a prototype that retains the fundamental elements of active-dissipative nonlinear media: the dominant nonlinear term (HH_X), instability (H_{XX}) arising here from inertia surface tension through the curvature of the fibre, stability (H_{XXXX}) here due to surface tension through the curvature of the interface, and dispersion (δH_{XXX}) promoted here by viscous effects. We assume that H can be written as a superposition of n quasi-stationary pulses $H_1, \ldots, H_n$ located at $X_1(T), \ldots, X_n(T)$, respectively, and a small overlap function, $\hat{H}$, i.e. $H = \sum_{i=1}^{n} H_i + \hat{H}$. We consider weak interaction assuming that the pulses are sufficiently separated and, therefore, for each pulse it is sufficient to take into account its interaction with only the immediate neighbors. We

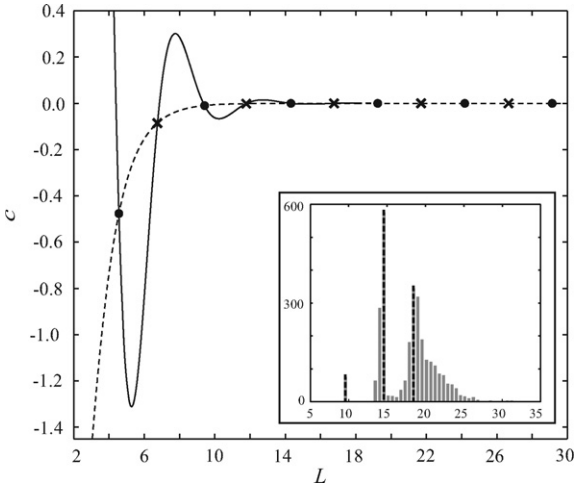

Fig. 7. Dependence of S_1 (dashed line) and S_2 (plain line) on the separation distance between pulses L for $\delta = 0.4$; • – stable bound state, × – unstable bound state. Subplot: histogram of the pulse separation distances obtained numerically by solving system (4).

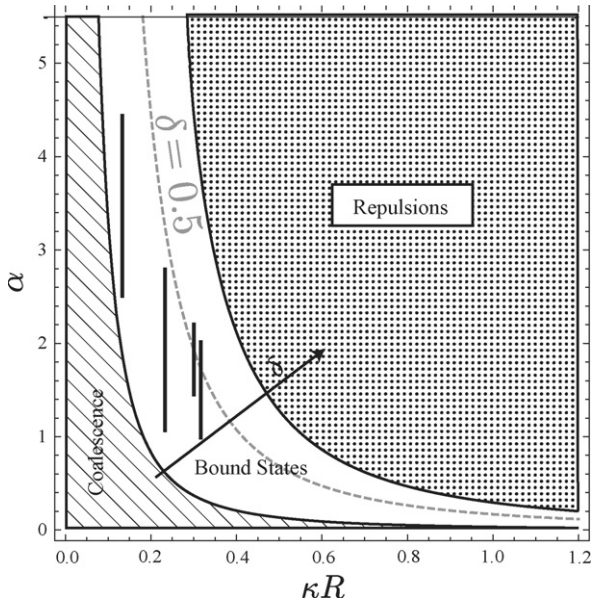

Fig. 8. Map of the different regimes in the plane ($\alpha = h_0/R$, κR). The bottom-left shaded region is defined by $\delta \leq 0.1$ and represents the dissipative regime where coalescence occurs. The top-right dotted region is defined by $\delta \geq 1$ and represents the dispersive regime where interactions are repulsive. The white region corresponds to intermediate values of δ for which both attractions and repulsions occur and bound states can be formed. The dashed grey line corresponds to the locus $\delta = 0.5$. Dark vertical segment show the range of values of (α, κR) at which bound states were observed experimentally.

then arrive at the following system describing the leading-order dynamics of the locations of the pulses (details are given in [5]):

$$\begin{aligned} X_1' &= S_1(X_2 - X_1), \\ X_i' &= S_2(X_i - X_{i-1}) + S_1(X_{i+1} - X_i); \quad 1 \leq i \leq n, \\ X_n' &= S_2(X_n - X_{n-1}), \end{aligned} \tag{4}$$

where S_2 and S_1 represent the interaction of the ith pulse with the oscillatory front of the upstream pulse $(i-1)$ and with the monotonic tail of the downstream pulse $(i+1)$, respectively. We now consider the interaction of two pulses separated by a distance $X_2 - X_1 = L$. From Eq. (4), $S_{1,2}$ now represent the speeds $c_{1,2}$ of the pulses in the moving frame at speed c_δ, that is $X_1' = c_1 = S_1(L)$ and $X_2' = c_2 = S_2(L)$. The variation of $S_{1,2}$ as a function of the pulse separation distance L is shown in Fig. 7 for $\delta = 0.4$.

Depending on their initial separation distance L, pulses can attract or repel each other corresponding to stable or unstable separation distances. For example, let us take $L_1 \approx 11$. In this case, $S_1 > S_2$, hence $c_1 > c_2$, the upstream pulse 1 travels faster than the downstream pulse 2, hence they two pulses approach each other (L decreasing) so that the velocity difference between the two decreases until both pulses travel at the same velocity, forming a bound state (with $L = 9.5 < L_1$). For $L = 8$, $S_2 > S_1$ and the pulses repel each other ($c_1 < c_2$): L increases until pulses form a bound state with $L = 9.5$ (> 8). The distances at which bound states can be formed are then given by the abscissas of the intersections of S_1 and S_2. For $\delta \lesssim 0.85$, there is a countable infinite number of intersections of S_1 and S_2 (but in time-dependent computations, to be described below, the system selects a finite number of distances corresponding to the smaller intersections). S_2 is oscillatory approaching a sinusoidal function for $L \gtrsim 6$ while S_1 levels off quickly with L, so that their intersections are located at distances which have a common factor, a feature that was evidenced in the experiments. On the other hand, the distance $L \approx 7$ is unstable to small displacements: $L \gtrsim 7$ (resp. $L \lesssim 7$) leads to $c_2 > c_1$ (resp. $c_1 > c_2$), hence repulsion (resp. attraction) that is L increases (resp. decreases) away from the value 7.

We have solved numerically (4) for two pulses and $\delta = 0.4$ and studied the evolution of a large average number of pulses with the initial distance distribution taken normal. We observed both attraction and repulsion, as well as formation of 2-pulse and 3-pulse bound states. The resulting histogram of the large-time separation distances is given in the insert of Fig. 7. We observe three peaks formed at $\simeq$9.5, 14 and 18.5, which are in very good agreement with the stable two-pulses bound state distances given by the intersections of S_1 and S_2. However, converting the dimensionless distances 9.5, 14 and 18.5 to dimensional ones, gives 0.42 cm, 0.62 cm and 0.82 cm. When compared with the preferred distances obtained experimentally for $\delta = 0.4$ ($L_1 \approx 1.2$ cm, $L_2 \approx 1.8$ cm and $L_3 \approx 2.6$ cm), we find that the experimental distances are larger than the theoretical ones by a factor of $\simeq$3. Hence, we do not have a quantitative agreement on the distances but this should be expected as for the theory R was assumed to be large compared to h_0, which is not the case in the experiments (where $\alpha = O(1)$). Nevertheless, we have a good qualitative agreement on many features present in the experiments, i.e. that pulses can form bound states via both attraction and repulsion, and that the system appears to select a certain number of distances which have a common factor. The formation of bound states is precisely due to the overlap of the front/back tails of successive pulses. Our theory also emphasizes the significance of the dispersion parameter δ. When $\delta \gtrsim 1$[1] (or $\delta \lesssim 0.1$), the system is purely dispersive (resp. dissipative), waves do not have any frontal ripples (they have large amplitude frontal oscillations, resp.) and no bound states can be observed, interactions being only repulsive (resp. attractive with deep inelastic coalescence events leading to spatio-temporal chaos). As noted earlier, the theory also suggests that depending on their initial separation distance, the pulses will lock on at the nearest distance corresponding to a stable bound state, in agreement with the experiments. In the experiments for the natural (unforced) case the initial distance distribution is broad, as it arises from the random destabilization of the primary wave train. On the other hand, in the experiments for the forced case, pulses are initially placed at distances closer to their equilibrium values and as a result the pulses rearrange themselves rapidly.

[1] The <fn0005>coherent structures theory predicts a finite number of intersections for $0.85 \lesssim \delta \lesssim 1.3$ and no intersections for $\delta \gtrsim 1.3$. But numerical experiments with the gKS equation show no bound states for $\delta \gtrsim 1$.

We are now in a position to construct a regime map that summarizes our results and which is presented in Fig. 8. The bottom-left shaded region is defined by $\delta \leq 0.1$ and represents the dissipative regime, the top right dotted region is defined by $\delta \geq 1$ and represents the dispersive regime while the white region corresponds to intermediate values of δ for which both attractions and repulsions occur and bound states can be formed. Experimentally, bound states were observed for all experimentally reachable thickness on four fibre radii $R = 0.2$,0. 35, 0.45, 0.475 mm, that is for $0.13 < \delta < 0.52$. Bound states were never observed on a larger fibre radius ($R = 1.5$ mm) for which reachable thicknesses give $\delta > 1$. Smaller values of δ cannot be obtained in our experiment as we cannot reach a thickness below the critical film thickness of $\simeq$0.5 mm for which no flat film can emerge from the meniscus at the entrance valve: the instability grows faster that the time necessary to form the meniscus which breaks instantaneously into droplets, leading to dripping of the liquid from the faucet (referred to as "regime c" by Kliakhandler et al. [2]). It is interesting to note that no bound states were noticed in experiments performed on a planar substrate ($\kappa R > 1$) and for less viscous fluids (water or alcohol) for which $\delta < 0.1$ [9]. These observations indicate that δ is indeed the right parameter to describe wave interactions on a liquid film coating a vertical fibre and allow us to determine whether surface tension (leading to large capillary ripples, hence attractions) or viscosity (damping the ripples leading to repulsions) dominates.

4. Conclusion

In this study, we have provided evidence for bound-state formation phenomena in low-Reynolds number interfacial hydrodynamics. More specifically, we have investigated experimentally pulse interactions on a viscous film coating a vertical fibre and demonstrated that in a certain regime of the parameter space, the flow organizes into a series of bound states. A rigorous coherent structures theory for a simple model of the flow, the gKS equation, explains the observed phenomena qualitatively.

References

[1] A.L. Frenkel, Europhys. Lett. 18 (1992) 583;
S. Kalliadasis, H.-C. Chang, J. Fluid Mech. 261 (1994) 136.
[2] I.L. Kliakhandler, S.H. Davis, S.G. Bankoff, J. Fluid Mech. 249 (2001) 381.
[3] C. Duprat, C. Ruyer-Quil, S. Kalliadasis, F. Giorgiutti-Dauphiné, Phys. Rev. Lett. 98 (2007) 244502;
C. Ruyer-Quil, P. Treveleyan, F. Giorgiutti-Dauphiné, C. Duprat, S. Kalliadasis, J. Fluid Mech. 603 (2008) 431.
[4] C. Ruyer-Quil, P. Treveleyan, F. Giorgiutti-Dauphiné, C. Duprat, S. Kalliadasis, Eur. Phys. J. Special Top. 166 (2009) 89.
[5] C. Duprat, F. Giorgiutti-Dauphiné, D. Tseluiko, S. Saprykin, S. Kalliadasis, Phys. Rev. Lett. 103 (2009) 234501.
[6] C. Duprat, C. Ruyer-Quil, F. Giorgiutti-Dauphiné, Phys. Fluids 21 (2009) 042109.
[7] T. Kawahara, Phys. Rev. Lett. 51 (1983) 381;
C.M. Alfaro, R.D. Benguria, M.C. Depassier, Physica D 61 (1992) 1;
C.I. Christov, M.G. Velarde, Physica D 86 (1995) 323.
[8] L.E. Ballentine, Quantum Mechanics: A Modern Development, World Scientific, Singapore, 1998;
K. Drescher, K.C. Leptos, I. Tuval, T. Ishikawa, T.J. Pedley, R.E. Goldstein, Phys. Rev. Lett. 102 (2009) 168101;
G.A. Voth, B. Bigger, M.R. Buckley, W. Losert, M.P. Brenner, H.A. Stone, J.P. Gollub, Phys. Rev. Lett. 88 (2002) 234301;
A.B. Ezersky, S.V. Kiyashko, A.V. Nazarovsky, in: S. Boccaletti, et al. (Eds.), Experimental Chaos: 6th Experimental Chaos Conference, AIP, New York, 2002.
[9] J. Liu, J.P. Gollub, Phys. Fluids 6 (1994) 69–101.